Ultrasonics Sonochemistry 31 (2016) 417–422

Contents lists available at ScienceDirect

Ultrasonics Sonochemistry

journal homepage: www.elsevier.com/locate/ultson

Preparation of metal–ceramic composites by sonochemical synthesis of metallic nano-particles and in-situ decoration on ceramic powders

A. Poulia [a], P.M. Sakkas [a], D.G. Kanellopoulou [a], G. Sourkouni [b,c], C. Legros [d], Chr. Argirusis [a,b,c,*]

[a] National Technical University of Athens, School of Chemical Engineering, Laboratory of Inorganic Materials Technology, 15780 Athens, Greece
[b] Institut für Energieforschung und Physikalische Technologien, Clausthal University of Technology, Leibnizstr. 4, 38678 Clausthal-Zellerfeld, Germany
[c] Clausthaler Zentrum für Materialforschung (CZM), Agricola Str. 2, 38678 Clausthal-Zellerfeld, Germany
[d] Université Paris-Sud 11, Institut de Chimie Moléculaire et des Matériaux, 91405 Orsay Cedex, France

ARTICLE INFO

Article history:
Received 16 November 2015
Received in revised form 21 January 2016
Accepted 27 January 2016
Available online 28 January 2016

Keywords:
Ultrasound
Sonochemistry
Nanoparticles
Decoration
Metal–ceramic composites

ABSTRACT

Copper and nickel nanoparticles were synthesized using reducing agents in the presence of direct high energy ultra-sonication. The metallic nanoparticles were decorated on various ceramic substrates (e.g. α-Al_2O_3, and TiO_2) leading to metal reinforced ceramics with up to 45% metallic content. Different parameters, such as the amount of precursor material or the substrate, as well as the intensity of ultrasound were examined, in order to evaluate the percentage of final metallic decoration on the composite materials. All products were characterized by means of Inductively Coupled Plasma Spectroscopy in order to investigate the loading with metallic particles. X-ray Diffraction and Scanning Electron Microscopy were also used for further sample characterization. Selected samples were examined using Transmission Electron Microscopy, while finally, some of the powders synthesized, were densified by means of Spark Plasma Sintering, followed by a SEM/EDX examination and an estimation of their porosity.

1. Introduction

Nowadays, in most engineering and high-tech branches there is an urgent need for development of novel products with better properties and innovative functionalities. Ceramic Matrix Composites (CMC), incorporating metallic inclusions present improved properties, necessary in innovating applications. In the past two decades, considerable efforts were put on the synthesis and decoration of metallic particles on various ceramic substrates. The final composites have gained great interest due to their unusual properties and potential applications in catalytic, electronic and magnetic material field [1,2].

Recent advances in nanostructured composites have been led by the development of new synthetic methods such as photolytic reduction [3], sonochemical method [4], micro emulsion technique [5] and alcohol reduction [6] that provide control over size, morphology and nano or microstructure. Among these techniques, sonochemical processing has been proven to be a useful tool for generating novel materials with unusual properties [7].

The application of ultrasound covers different fields such as electro-plating, electro-organic synthesis, electro-polymerization, electro-analytical chemistry and the sonochemical synthesis of nanoparticles [8–11]. In this work we will focus on sonochemistry as a new, cost-effective and green method for the synthesis and decoration of metallic particles on various ceramic substrates.

Sonochemistry is the research area in which molecules undergo a chemical reaction due to the application of powerful ultrasound radiation (20 kHz–10 MHz). The chemical effects of ultrasound arise from a physical phenomenon known as acoustic cavitation. This phenomenon consists of the formation, growth, and implosive collapse of bubbles in the liquid, which invoke unusual chemical environments. The collapse of these bubbles, described as an adiabatic implosion in the hot-spot theory, is the origin of extreme local conditions, such as high temperature (more than 5000 K) and high pressure (up to 2000 bar). The cooling rates obtained following the collapse, are also greater than 10^{10} K s^{-1} [12,13], while the mean life time of the bubble does not exceed 300–400 μs. These extreme conditions attained during bubble collapse, allow the synthesis of nanoscale metals, metal oxides, and nanocomposites [14–16].

The first report on the use of ultrasound for the fabrication of noble metals was in 1987 by the work of Gutierrez et al. [17] followed by the work of Nagata et al. [18] in 1992 who studied the reduction of silver ions. Nanostructured metals were

* Corresponding author at: National Technical University of Athens, School of Chemical Engineering, Laboratory of Inorganic Materials Technology, 15780 Athens, Greece.
E-mail address: amca@chemeng.ntua.gr (Chr. Argirusis).

http://dx.doi.org/10.1016/j.ultsonch.2016.01.031
1350-4177/

sonochemically first prepared in non-aqueous solutions. For example, Suslick et al. developed a novel route to prepare amorphous iron metal and colloidal iron nanoparticles [12,13,19].

The effect of surfactants and their use during sonication also seemed to be a big concern for the research community. Okitsu et al. [20] studied the role of surfactants on the size of Pd nanoparticles and the sonochemical reduction mechanisms of Pd(II). Mizukoshi et al. [21] also investigated the effect of different surfactants on the sonochemical reduction of Pt(IV) ions.

In general, sonochemical synthesis produces spherical metal nanoparticles, and thus the process had been limited in preparing other metal nanostructures (e.g. nanorods, nanowires etc.). Recently, Han et al. [22] reported an intriguing result on shape control. In their synthetic approach, ultrasonic irradiation of an aqueous $HAuCl_4$ solution containing a-D-glucose produced gold nanobelts having a width of 30–50 nm and a length of several micrometers. Another shape control method using ultrasound was reported by Liz-Marzán et al. [23,24] who synthesized monodispersed gold nanodecahedra via ultrasound-induced reduction of $HAuCl_4$ in DMF solution. A similar synthetic strategy was also followed by Zhu et al. [25] in the synthesis of silver nanoplates.

Finally, the effect of different experimental parameters such as time, concentration and ultrasonic frequency on the particle size and shape is covered by a big part of the corresponding literature [7,26–32].

2. Experimental

2.1. Sonochemical synthesis of copper particles and decoration on ceramic substrates

The experimental procedure was based on the work of Tao et al. [33] followed by some variations in order to ensure the decoration of copper particles on the ceramic substrates. The basic steps of the sonochemical synthesis were the following: 2 g of L-ascorbic acid (reducing agent), 3.4 g of CTAB (dispersant), 1 g of the ceramic substrate (e.g. α-Al_2O_3 or TiO_2) and 75 ml of distilled water were added into a round bottom flask to form Solution 1 (S_1). Then, 1 g of the metal precursor $CuCl_2{\cdot}2H_2O$, 6 ml of NH_3 (pH regulator) and 15 ml of deionized water were used to form Solution 2 (S_2). An ultrasonic horn (20 kHz, 100 W/cm^2) was introduced in the flask containing S_1, thermo stated at 62 °C and irradiated for 30 min, generating a colorless and transparent fluid. S_2 was then added to S_1 in one single addition and the resultant mixed solutions, with a total volume of 100 ml, were additionally irradiated for 2 h. Finally, the precipitates were collected from the reaction system by centrifugation (3000 rpm) in glass tubes, washed thoroughly with deionized water and dried at 100 °C overnight.

Different amount ratios of the precursor and substrates (commercial α-Al_2O_3 1–5 micron powder supplied by Strem Chemicals, laboratory synthesized α-Al_2O_3 (annealed at 1200 °C) and commercial TiO_2 1077 supplied by Kronos with a specific area of 12 m^2/g), as well as changes in the intensity of ultrasound (100 and 30 W/cm^2) were examined as summarized in Table 1.

2.2. Sonochemical synthesis of nickel particles and decoration on ceramic substrates

Based on the work of Wu and Chen [34] the typical procedure in the case of nickel synthesis is briefed as follows: a certain amount of $NiCl_2{\cdot}6H_2O$ was dissolved in ethylene glycol and then hydrazine was added. An appropriate amount of NaOH was then added in order to adjust the solution pH and act as a catalyst. An ultrasonic horn (20 kHz, 100 W/cm^2) was introduced for 2 h in the flask containing the final solution, while the temperature was kept at 62 °C throughout the reaction, as it was found that the reaction was completed only at elevated temperature. The powder obtained was isolated by centrifugation (3000 rpm) in glass tubes, washed thoroughly with deionized water and dried at 100 °C overnight. The decoration of nickel particles on ceramic substrates, as well as its progress with time was further examined.

Table 1
Conditions for the sonochemically synthesized samples of Cu.

Sample code name	Precursor $CuCl_2{\cdot}2H_2O$ (g)	Ceramic substrate	Ultrasound intensity (W/cm^2)
C1	1.5	0.25 g lab/ry α-Al_2O_3 (1200 °C)	100
C2	1.5	1.0 g commercial α-Al_2O_3	100
C3	1.5	2.0 g commercial TiO_2	100
C4	1.5	–	100
C5	0.5	1.0 g commercial α-Al_2O_3	100
C6	1.0	1.0 g commercial α-Al_2O_3	100
C7	2.0	1.0 g commercial α-Al_2O_3	100
C8	1.0	1.0 g commercial α-Al_2O_3	30
C9	1.5	1.0 g commercial α-Al_2O_3	30
C10	0.5	2.0 g commercial α-Al_2O_3	100
C11	2.0	2.0 g commercial α-Al_2O_3	100

All samples were characterized by means of Inductively Coupled Plasma Spectroscopy (ICP-AES) and powder X-ray Diffraction techniques. Their microstructure was studied by Scanning Electron Microscopy (SEM) followed by EDX analysis. Selected samples were examined using Transmission Electron Microscopy (TEM), while some of the Cu/α-Al_2O_3 powders became dense by means of Spark Plasma Sintering (SPS) for their further characterization.

2.3. Spark Plasma Sintering

SPS experiments were carried out in a Dr. Sinter 515S Syntex apparatus. The powders were poured into a carbon die of 8 mm diameter, the internal face of which was covered with a thin graphite foil (papayex®) to avoid direct contact between the powder and the graphite die. The die was closed by carbon punches at both sides that are used as current contacts, as well as to apply uniaxial pressure. DC pulses were delivered to the die by the punches allowing the temperature of the die to rise rapidly. Graphite felt around the die was also used to reduce the heat loss by radiation. Sintering temperature was measured by an optical pyrometer focused on a small hole in the graphite die. For maximum reproducibility, the sintering temperature and pressure were controlled by automatic controller units. The samples were heated by applying pulsed direct current which passes through punch and die system. The pulse time duration was set at 3.3 ms, a pulse pattern consisted of 12 pulses each followed by a period of 6.6 ms during which no current was used. All experiments were conducted in vacuum of about 30 mbar.

To produce fully densified samples with a fine grain size, a two-steps sintering process was used. In all cases, the temperature was automatically raised to 600 °C within 1 min and kept constant for 6 min prior to the start of the experiment, during which it was monitored and regulated using a pyrometer. Afterwards samples were heated to the first step temperature T_1 = 1000 °C with a heating rate of 100 °C/min. As soon as the temperature T_1 was reached, a constant uniaxial pressure of 5 kN was applied on the die. The sample was maintained at this temperature for a first step sintering time of 20 min. The temperature was then increased, with the same heating rate, to the second sintering temperature T_2 = 1200 °C and hold there for 20 min. A rapid cooling, during which the pressure was linearly decreased, ended the sintering cycle. After sintering, the samples were cut, mounted and polished according to a specific preparation process for their further characterization.

3. Results and discussion

3.1. Copper decoration on ceramic substrates

The sonication of copper chloride precursor in an aqueous solution led to the formation of metallic copper nanoparticles, decorated on different ceramic substrates in one step.

The reduction of the copper ions is mainly due to the added reducing agent ascorbic acid [33]. From the time that copper nanoparticle synthesis experiments were run under continuous sonication in water with pH > 7, colloidal copper can be produced during water sonication through a reduction process involving species stemming from water decomposition [35] but only as side reaction. Sonication affects more the shape and distribution of the produced particles as well as their in-situ decoration of the substrates.

The mechanism, by which the decorated particles reached the ceramic substrate and their ability not to be removed, despite the severe stirring caused by the ultrasound wave, is quite complicated. When during sonication a bubble collapses near a solid surface, the formation of shock waves and micro-jets created as aftereffects, take place. These jets most likely push the ultrafine particles towards the solid surface of the substrates at very high speeds. Once the nanoparticles collide with the surface, chemical bond or weak interactions keep them on the surface in most cases.

The crystalline structure of the sonochemically prepared samples was examined by constructing the corresponding XRD patterns of Fig. 1. These plots represent three samples with the same amount of copper chloride as a precursor and different amounts and kinds of ceramic substrates. In all cases, the existence of the characteristic peaks of Cu and those of the substrates were observed, while no peaks of impurities (such as Cu_2O or CuO) were detected, giving a first sign that the products prepared, consisted of metallic Cu.

The microstructure of sonochemically prepared copper samples was further examined using Scanning Electron Microscopy. The microstructure of a decorated copper sample as captured by SEM, is presented in Fig. 2. This sample (C1) consists of 1.5 g $CuCl_2 * 6H_2O$ precursor and 0.25 g of laboratory synthesized α-Al_2O_3 (1200 °C) as a substrate. The existence of mainly disk-like copper particles as well as some rods, both of which seem to be agglomerated, is evident. The size of the agglomerated primary particles ranges at the scale of nanometers, while an EDX mapping analysis proved the absence of copper oxides formed during the specific sonochemical synthetic route.

As already mentioned, the loading percentage of copper was estimated in all samples by means of ICP-AES, after the powders digestion. In Fig. 3a and b the diagrams presenting, show the influence of metal precursor amount and the changes in the ultrasound intensity on the final decoration of the products.

Fig. 3a shows the influence of the amount of copper chloride precursor on four different samples consisting of the same amount of 1 g commercial α-Al_2O_3 as a substrate. It is clear that as the amount of the precursor increases, the corresponding copper wt% loading also increases. The use of at least 1 g of $CuCl_2{\cdot}2H_2O$ seems to be vital in order to achieve a 35% of Cu decoration, while in most cases, the 2 h of sonication proved to be enough for a desirable Cu loading around 35–45%.

Fig. 3b presents the influence of the intensity changes (from 100 to 30 W/cm^2) for two groups of samples consisting of 1.0 g and 1.5 g of commercial α-Al_2O_3 as substrate and different amounts of copper precursor, respectively. In both cases a slight decrease in the percentage of copper decoration, as the intensity decreases from 100 to 30 W/cm^2 is observed. In both cases though, even with the use of the lower intensity, a copper decoration above 28% was achieved. This observation is quite important for the use of lower ultrasound intensity and how it influences the sonochemical decoration of metallic particles on ceramic substrates.

As already mentioned, selected samples of decorated copper on alumina substrate, became dense by means of SPS. Fig. 4a and b present the SEM microstructures of two samples consisting of 0.5 g $CuCl_2{\cdot}2H_2O$ – 2 g of commercial α-Al_2O_3 and 2.0 g of $CuCl_2{\cdot}2H_2O$ – 2 g of commercial α-Al_2O_3 as substrate, respectively. In both cases, the existence of copper particles (white spots), as well as the α-Al_2O_3 grains (gray areas), are evident. In the first sample (C10) the Cu wt%, before SPS, was estimated via SEM/EDX at 0.58%, while after SPS it further decreased to 0.24% due to copper melting near the die walls. An increase of the Cu grain size was also observed. Before sintering, the initial Cu grain size was around 1 μm, while after SPS it ranged around 10 μm. With the use of an optical microscope the porosity of the specific sample was estimated around 1%.

In the second sample C11 (with a higher amount of copper decoration), the Cu particles and the area corresponding to the substrate are also spotted. The percentage of Cu before SPS was measured at 18.6%, while after SPS it decreased to 12.1%. The

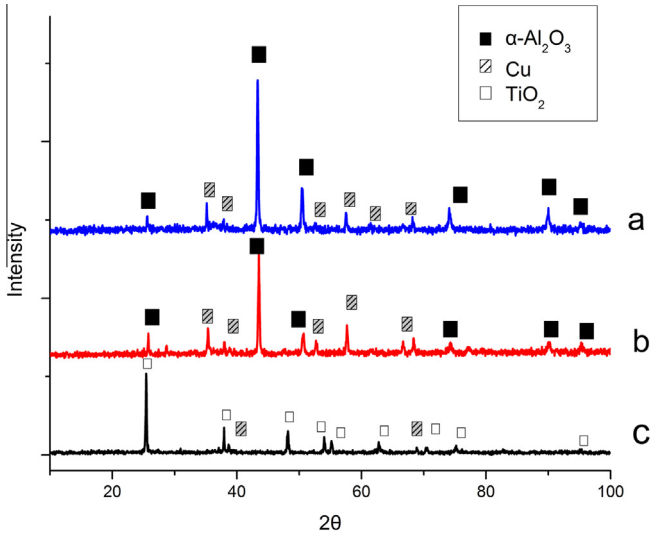

Fig. 1. Powder XRD patterns of (a) 1.5 g copper precursor – 0.25 g laboratory synthesized a-Al_2O_3 (1200 °C) as substrate (Sample C1), (b) 1.5 g copper precursor – 1.0 g commercial a-Al_2O_3 as substrate (Sample C2) and (c) 1.5 g copper precursor – 2.0 g commercial TiO_2 as substrate (Sample C3).

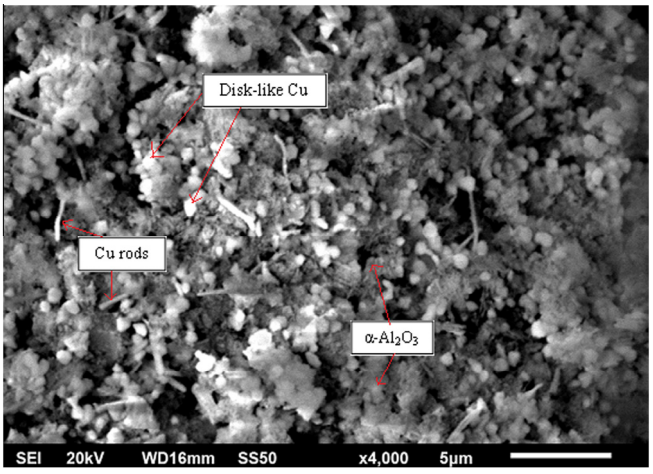

Fig. 2. SEM microstructures of sample C1 consisting of 1.5 g copper precursor and 0.25 g of laboratory synthesized a-Al_2O_3 (1200 °C) as a substrate.

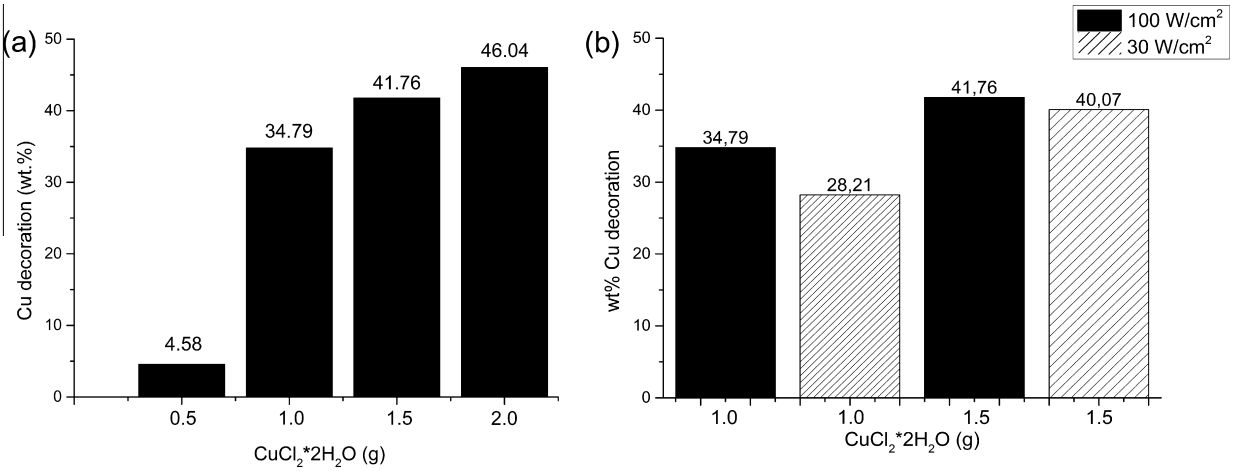

Fig. 3. (a) ICP-AES results regarding the influence of 0.5, 1.0, 1.5 and 2.0 g of metal precursor on 1 g of commercial a-Al_2O_3 (Samples C5, C6, C2 and C7, respectively) (b) ICP-AES results regarding the influence of the US intensity changes for Samples C6, C8, C2 and C9 respectively.

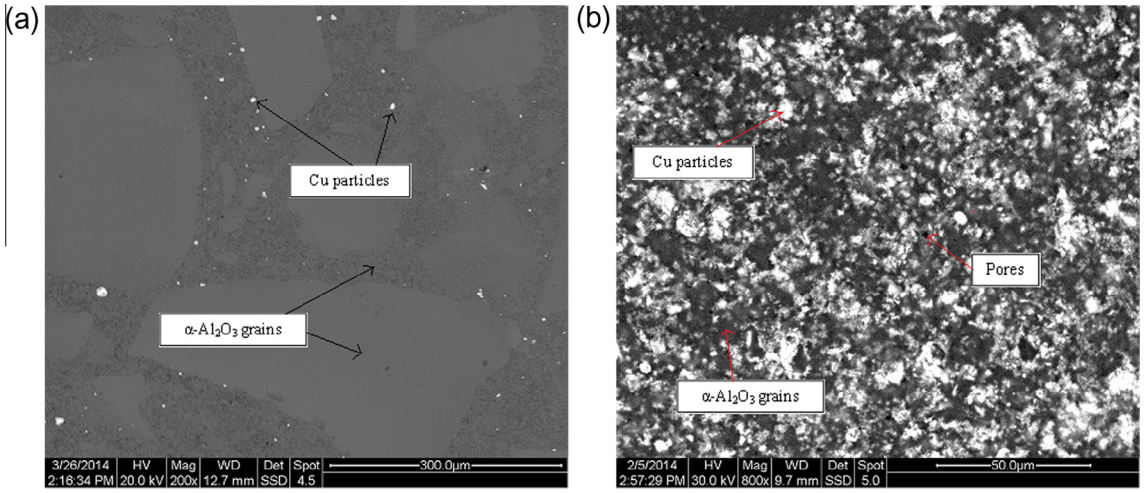

Fig. 4. a and b. SEM images after SPS for Samples C10 and C11 consisting of 0.5 g and 2.0 g of $CuCl_2{\cdot}2H_2O$ and 2.0 g of commercial α-Al_2O_3 as substrate, respectively.

percentage of reduction was estimated around 35%. Finally, the porosity of sample C11 slightly increased, in comparison to the previous sample, reaching a percentage of 3.5%. The increase of the percentage of copper caused a decrease of the corresponding resistance through the sample and worked against the densification process for samples leading to the slightly higher porosity.

In general, evaluating the sintering results, it was clear that the increase of copper loading on the ceramics enabled densification through Spark Plasma Sintering. Pure alumina samples, as non-electrically conductive ceramics, did not seem to be influenced by the heating rate, the pressure or the DC during SPS process. On the other hand, the addition of copper to the final composites seemed to change things drastically as copper, which over a temperature range becomes more ductile, densified easier even only due to the compression.

Finally, a TEM image is presented in Fig. 5 which shows the micrograph of sample C3 consisting of 1.5 g $CuCl_2{\cdot}2H_2O$ and 2 g of commercial TiO_2 as substrate. As observed, TiO_2 crystallites consist of 100% anatase with dimensions between 100 and 110 nm, while copper particles with a mean diameter around 5 nm seem to be well distributed and successfully decorated on the surface of the ceramic material.

3.2. Nickel decoration on ceramic substrates

The sonication of nickel chloride precursor in an organic solution led to the formation of metallic nickel particles, decorated on different ceramic substrates. In the current investigation, ultrasonic waves served as a source of energy to drive the reactions. The preparation of nickel particles was based on a reduction mechanism using a certain amount of hydrazine as a reducing agent. The stability of the synthesized nickel is probably due to the presence of free polymer chains of ethylene glycol and hydrazine. The viscosity of these organic solvents probably plays an important role in the stabilization mechanism of the nickel formation. It restricts diffusion of the particles through the dispersion medium and leads to their successful synthesis and decoration on ceramic substrates.

Once again, the crystalline structure of the sonochemically prepared samples was examined by X-ray Diffraction. The following patterns of Fig. 6 correspond to two different samples. The first one (sample N1) consists of pure nickel (0.23 g of $NiCl_2 * 6H_2O$ as a metal precursor without a ceramic substrate), while the second one (sample N2) has the same amount of nickel precursor and 0.25 g of commercial α-Al_2O_3 as substrate.

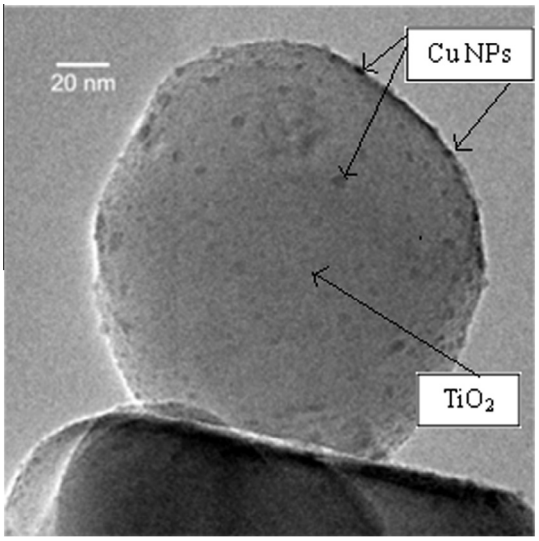

Fig. 5. TEM images of sample C3 consisting of 1.5 g $CuCl_2{\cdot}2H_2O$ and 2 g of commercial TiO_2 as substrate.

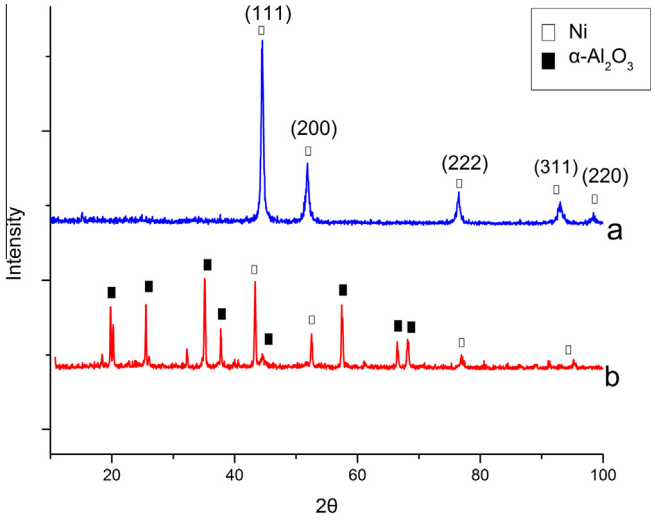

Fig. 6. Powder XRD patterns of (a) Sample N1 and (b) Sample N2 consisting of 0.23 g of $NiCl_2 * 6H_2O$ as a metal precursor without a ceramic substrate and with 0.25 g of commercial a-Al_2O_3 as substrate, respectively.

The three characteristic peaks of nickel ($2\theta = 44.5°$, 51.8° and 76.4°) correspond to Miller indices (111), (200) and (222). The resultant particles were pure face-centered cubic (fcc) nickel. The sharp shape of the peaks indicates the crystalline nature of the particles synthesized, while the absence of oxides or hydroxides such as NiO or $Ni(OH)_2$, is attributed to the fact that the reaction was performed in an organic solvent.

The microstructure of the sonochemically synthesized nickel particles of sample N1 is presented in Fig. 7.

As shown, the microstructure of the sonochemically synthesized nickel particles presents two morphologies: Firstly, the existence of mainly nickel rods with some nickel disks placed on their edges is clear. Furthermore, the formation of fewer nickel dendrites spotted between the rods is evident. Moreover, a better look on a Ni dendrite reveals the existence of individual spherical Ni nanoparticles that form the wider dendritic configurations.

The successful synthesis of nickel nanoparticles was also verified by TEM. Fig. 8 presents the microstructure of sample N2 (0.23 g of $NiCl_2 * 6H_2O$ – 0.25 g of commercial α-Al_2O_3 as substrate)

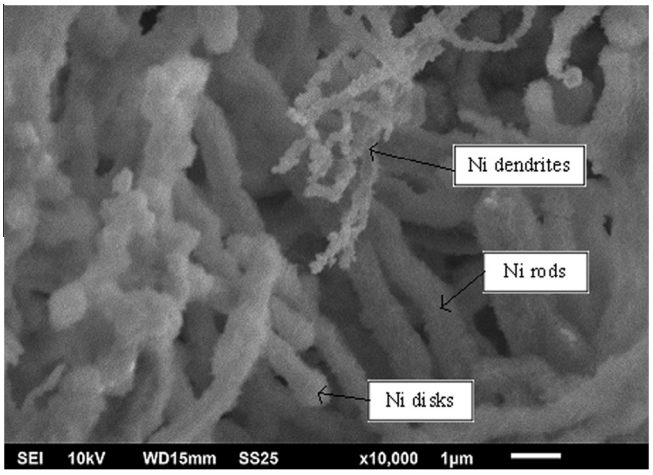

Fig. 7. SEM micrograph of the sonochemically synthesized sample N1 consisting of 0.23 g of $NiCl_2 * 6H_2O$ as a metal precursor without a ceramic substrate.

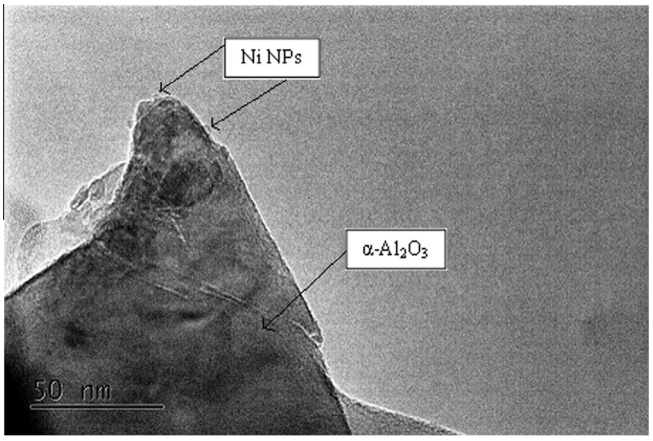

Fig. 8. TEM image of the decorated nickel particles on the α-Al_2O_3 substrate (sample N2).

Table 2
Conditions for the sonochemically synthesized samples of Ni.

Sample code name	Precursor $NiCl_2{\cdot}6H_2O$ (g)	Ceramic substrate	Ultrasound intensity (W/cm^2)
N1	0.23	–	100
N2	0.23	0.25 g commercial α-Al_2O_3	100

(See Table 2). Nickel nanoparticles with a size around 5 nm are successfully decorated on the α-Al_2O_3 grains.

Finally, the decoration progress with time, during the sonochemical synthesis of nickel nanoparticles was examined by means of ICP-AES after centrifugation and powder digestion. In order to achieve this, a specific amount of the sonicated sample was taken from the flask every 20 min during the 2 h irradiation.

By evaluating the corresponding data, it was made clear that even in the first 20 min of the sonication a desirable nickel loading around 40% was achieved. Since then and until the end of the 2 h of sonication, no drastic changes were spotted in the percentage of Ni decoration. It is also worth mentioning that from the beginning (20 min) until the end (120 min) of the sonication the percentage of Ni decoration was always kept above 35%. This result is quite important as it reveals that the duration of the sonication could

be smaller, without dramatically influencing the decoration percentage of the metallic particles on the ceramic substrate, ensuring several functional and economic benefits for the US apparatus.

However, the small deviations of the decoration values, which would probably lead to a saturation threshold if the time of sonication was larger, can be attributed to different aspects. For example, the increase of the decoration values may be caused by the beneficial effect of ultrasounds which "load" the substrate and manage to decorate the free particles of the sonicated slurry. On the other hand, the small decreases of the decoration values can be attributed to the following reasons. Firstly, it is possible that the extreme conditions caused by the acoustic cavitation during sonication could "damage" the decoration process and act in a competitive way, leading to a breakdown of the decorated particles. Secondly, it is also possible that, under these circumstances, the successfully decorated nanoparticles, could "break" into smaller ones, thus making them impossible to be calculated by means of ICP-AES.

4. Conclusions

Copper and nickel metallic nanoparticles were synthesized using reducing agents in presence of direct high energy ultrasonication successfully decorated in-situ on various ceramic substrates (e.g. commercial and laboratory α-Al_2O_3 and commercial TiO_2). The XRD patterns revealed, in both cases, the formation of pure metallic particles with high crystallinity. SEM images showed the existence of mainly disk-like copper particles and a small amount of rods, which seemed to act as bridges connecting the disk-like particles. In the case of nickel, the formation of some dendritic configurations was also spotted. The choice of Spark Plasma Sintering proved to be a good option for the densification of Cu–α-Al_2O_3 powders, while the TEM images verified the existence of copper and nickel nanoparticles successfully decorated on the corresponding ceramic substrates. A possibility of reducing the time of sonication without adversely influencing the decoration values was also proved.

Acknowledgements

This work was funded by the Greek Ministry of Education and Religious Affairs and the European Commission in the frame of the ESPA project entitled "Thalis – NTUA" – "*Development of nanostructured composite materials with ceramic matrix and metallic incorporations*". The authors are grateful to Professor A. Avgeropoulos and Assistant Professor A. Karantzalis from University of Ioannina, Greece for their assistance with TEM and SEM images, respectively, Mrs. M. Stucchi from Università Degli Studi di Milano, Italy for assistance with TEM images and Mrs. F. Petrakli from National Technical University of Athens, Greece for providing the laboratory synthesized α-Al_2O_3 powder. We are also indebted to the unknown reviewers for their valuable comments.

References

[1] B.C. Gates, Supported metal clusters: synthesis, structure, and catalysis, Chem. Rev. 95 (1995) 511–522.
[2] L.L. Beecroft, C.K. Ober, Nanocomposite materials for optical applications, Chem. Mater. 9 (1997) 1302–1317.
[3] S. Remita, M. Mostafavi, M.O. Delcourt, Bimetallic AgPt and AuPt aggregates synthesized by radiolysis, Radiat. Phys. Chem. 47 (1996) 275–279.
[4] P. Jeevanandam, Y. Koltypin, A. Gedanken, Synthesis of nanosized -nickel hydroxide by a sonochemical method, Nano Lett. 1 (2001) 263–266.
[5] K. Osseo-Asare, F.J. Arriagada, Synthesis of nanosize silica in a nonionic water-in-oil microemulsion: effects of the water/surfactant molar ratio and ammonia concentration, J. Colloid Interface Sci. 211 (1999) 210–220.
[6] H.H. Huang, X.P. Ni, G.L. Loy, Photochemical formation of silver nanoparticles in poly(N-vinylpyrrolidone), Langmuir 12 (1996) 909–912.
[7] R.A. Caruso, M. Ashokkumar, F. Grieser, Sonochemical formation of gold sols, Langmuir 18 (2002) 7831–7836.
[8] R.G. Compton, J.C. Eklund, F. Marken, Sonoelectrochemical processes: a review, Electroanalysis 9 (1997) 509.
[9] C.E. Banks, R.G. Compton, Voltammetric exploration and applications of ultrasonic cavitation, Chem. Phys. Chem 4 (2003) 169–178.
[10] B. Pollet, Power Ultrasound in Electrochemistry: From Versatile Laboratory Tool to Engineering Solution, Wiley, Chichester, 2012.
[11] P. Sakkas, O. Schneider, S. Martens, P. Thanou, G. Sourkouni, Chr. Argirusis, Fundamental studies of sonoelectrochemical nanomaterials preparation, J. Appl. Electrochem. 42 (2012) 763–777.
[12] K.S. Suslick, S.-B. Choe, A.A. Cichowlas, M.W. Grinstaff, Sonochemical synthesis of amorphous iron, Nature 353 (1991) 414–416.
[13] M.W. Grinstaff, A.A. Cichowlas, S.-B. Choe, K.S. Suslick, Effect of cavitation conditions on amorphous metal synthesis, Ultrasonics 30 (1992) 168–172.
[14] K.S. Suslick, M.M. Fang, T. Hyeon, M.M. Mdleleni, Applications of sonochemistry to materials synthesis, Sonochem. Sonoluminescence (1999) 291–320.
[15] V.G. Kumar, K.B. Kim, Organized and highly dispersed growth of MnO_2 nanorods by sonochemical hydrolysis of Mn(3) acetate, Ultrason. Sonochem. 13 (2006) 549–556.
[16] C.J. Mao, H.C. Pan, X.C. Wu, J.J. Zhu, H.Y. Chen, Sonochemical route for self-assembled V_2O_5 bundles with spindle-like morphology and their novel application in serum albumin sensing, J. Phys. Chem. B 110 (2006) 14709–14713.
[17] M. Gutierrez, A. Henglein, J.K. Dohrmann, Hydrogen atom reactions in the sonolysis of aqueous solutions, J. Phys. Chem. 91 (1987) 6687–6690.
[18] Y. Nagata, Y. Watananabe, S. Fujita, T. Dohmaru, S. Taniguchi, Formation of colloidal silver in water by ultrasonic irradiation, J. Chem. Soc. Chem. Commun. (1992) 1620–1622.
[19] K.S. Suslick, M. Fang, T. Hyeon, Sonochemical synthesis of iron colloids, J. Am. Chem. Soc. 118 (1996) 11960–11961.
[20] K. Okitsu, H. Bandow, Y. Maeda, Sonochemical preparation of ultrafine palladium particles, Chem. Mater. 8 (1996) 315–317.
[21] Y. Mizukoshi, E. Takagi, H. Okuno, Preparation pf platinum nanoparticles by sonochemical reduction of Pt(IV) ions: role of surfactants, Ultrason. Chem. 8 (2001) 1–6.
[22] J. Zhang, J. Du, B. Han, Z. Liu, T. Jiang, Z. Zhang, Sonochemical formation of single-crystalline gold nanobelts, Angew. Chem. Int. Ed. 45 (2006) 1116–1119.
[23] A. Sánchez-Iglesias, I. Pastoriza-Santos, J. Pérez-Juste, B. Rodríguez-González, F. J. García de Abajo, L.M. Liz-Marzán, Synthesis and optical properties of gold nanodecahedra with size control, Adv. Mater. 18 (2006) 2529–2534.
[24] I. Pastoriza-Santos, A. Sánchez-Iglesias, F.J. García de Abajo, L.M. Liz–Marzán, Environmental optical sensitivity of gold nanodecahedra, Adv. Funct. Mater. 17 (2007) 1443–1450.
[25] L.P. Jiang, S. Xu, J.M. Zhu, J.R. Zhang, J.J. Zhu, H.Y. Chen, Ultrasonic-assisted synthesis of monodisperse single-crystalline silver nanoplates and gold nanorings, Inorg. Chem. 43 (2004) 5877–5883.
[26] K. Okitsu, M. Ashokkumar, F. Grieser, Sonochemical synthesis of gold nanoparticles: effects of ultrasound frequency, J. Phys. Chem. B 109 (2005) 20673–20675.
[27] K. Vinodgopal, Y. He, M. Ashokkumar, F. Grieser, Sonochemically prepared platinum-ruthenium bimetallic nanoparticles, J. Phys. Chem. B 110 (2006) 3849–3852.
[28] A. Brotchie, F. Grieser, M. Ashokkumar, Effect of water-soluble solutes on sonoluminescence under dual-frequency sonication, J. Phys. Chem. C 112 (2008) 10247–10250.
[29] S. Anandan, F. Grieser, M. Ashokkumar, Sonochemical synthesis of Au-Ag core-shell bimetallic nanoparticles, J. Phys. Chem. C 112 (2008) 15102–15105.
[30] Y. He, K. Vinodgopal, M. Ashokkumar, F. Grieser, Sonochemical synthesis of ruthenium nanoparticles, Res. Chem. Int. 32 (2006) 709–715.
[31] D. Radziuk, H. Mohwald, D. Shchukin, Sonochemical design of engineered gold-silver nanoparticles, J. Phys. Chem. C 112 (2008) 2462–2468.
[32] C. Wu, B.P. Mosher, T. Zeng, Rapid synthesis of gold and platinum nanoparticles using metal displacement reduction with sonomechanical assistance, Chem. Mater. 18 (2006) 2925–2928.
[33] X. Tao, Lei Sun, Y. Zhao, Sonochemical synthesis and characterization of disk-like copper microcrystals, Mater. Chem. Phys. 125 (2011) 219–223.
[34] S.H. Wu, D.H. Chen, Synthesis and characterization of nickel nanoparticles by hydrazine reduction in ethylene glycol, J. Colloid Interface Sci. 259 (2003) 282–286.
[35] T.J. Mason, J.P. Lorimer, Applied Sonochemistry: The uses of Power Ultrasound in Chemistry and Processing, Willey-VCH Verlag GmbG, Weinheim, 2002.